TITLE: **Optimised scanning strategy for the LFI-only extension**

DOC. TYPE: **TECHNICAL NOTE**

PROJECT REF.: **PL-LFI-PST-TN-099** PAGE: **I of IV, 12**

ISSUE/REV.: **Issue 1.2** DATE: **July 2012**

Prepared by	**See author list at beginning of Technical note**	**Date:** **Signature:**	**July, 2012**
Agreed by	**C. BUTLER** **LFI Program Manager**	**Date:** **Signature:**	**July, 2012**
Approved by	**N. MANDOLESI** **LFI Principal Investigator**	**Date:** **Signature:**	**July, 2012**

DISTRIBUTION LIST

Recipient	Company / Institute	E-mail address	Sent

CHANGE RECORD

Issue	Date	Sheet	Description of Change	Release
Issue 1.0	Oct '11	All	First issue of document	1.0

TABLE OF CONTENTS

Authors

Carlo Burigana (IASF-BO), Marco Bersanelli (UniMi), Anna Bonaldi (MAN), Mauro Casale (ESA), Francesco Cuttaia (IASF-BO), Richard Davis (MAN), Xavier Dupac (ESA), Fabio Finelli (IASF-BO), Steve Foley (ESA), Bruno Gandolfo (ESA), Joaquin Gonzalez-Nuevo (SISSA), Krzysztof Gorski (JPL), Anna Gregorio (UNI-TS), Alessandro Gruppuso (IASF-BO), Charles Lawrence (JPL), Samuel Leach (SISSA), Patrick Leahy (MAN), Nazzareno Mandolesi (IASF-BO), Michele Maris (OATS), Luis Mendes (ESA), Aniello Mennella (UniMi), Riccardo Miniscalco (ESA), Gianluca Morgante (IASF-BO), Adam Moss (UBC), Paolo Natoli (IASF-BO), Francois Pajot (IAS), David Pearson (JPL), Gianluca Polenta (ASI), Jean-Loup Puget (IAS), Sara Ricciardi (IASF-BO), Maura Sandri (IASF-BO), Douglas Scott (UBC), Anna-Stiina Suur-Uski (HEL), Laurent Vibert (IAS), Jan Tauber (ESA), Luca Terenzi (IASF-BO), Tiziana Trombetti (IASF-BO), Fabrizio Villa (IASF-BO), Chris Watson (ESA), Andrea Zacchei (OATS)

Abstract

The main reason for the extension of the *PLANCK* mission beyond the lifetime of the 0.1-K dilution cooler is to obtain further data which will improve our understanding of systematic effects. In the present report, we justify the continuation of the current scanning strategy in order to obtain a sixth survey, allowing for better sensitivity and further "jackknife" (survey difference) tests. The fifth survey is already improving the estimates of the polarisation leakage for two of the LFI horns, and this improvement will continue with the sixth survey during the extension. In addition, we confirm the "deep rings" scanning strategy to improve mapping of the beams using radio sources, specifically Jupiter and the Crab Nebula. We propose to maintain the current spin rate: no other changes are foreseen, except the possibility to increase the sampling of some house-keeping data.

1 Introduction

Since the start of the nominal survey on 15 August 2009, the *PLANCK* satellite has been observing the sky continuously, producing an exciting data set under very stable spacecraft and instrumental conditions. The original mission duration of fifteen months was first extended by twelve months (ESA/SPC(2009)25) up to the end of the expected lifetime of the 0.1-K dilution cooler, which determines the operational life of the High Frequency Instrument (HFI). After completion of the first two surveys, it became clear that the duration of the 4-K and 20-K coolers would exceed the lifetime of the 0.1-K dilution cooler, thus opening up the possibility of an extension of the *PLANCK* mission using only the Low Frequency Instrument (LFI) detectors.

In September 2010, the LFI Consortium, supported by the *PLANCK* Science Team, submitted a proposal (referred here as LOEP, the "LFI-Only Extension Proposal") to extend the operation of *PLANCK* in the so-called "LFI-only" mode for up to an additional year of observation. The proposal was approved by ESA (see ESA/SPC(2010)21 and Annexes) and it is now part of the baseline plan.

In the approved LOEP proposal, the scientific case was based, first and foremost, on the need for LFI to understand and remove systematic effects, and to improve calibration accuracy. These measurements, while carried out by the LFI detectors, were aimed at an enhanced analysis of the *PLANCK* data as a whole. In particular, we identified four main instrument-related aspects that would benefit from the "LFI-only" phase: 1. Optical beam measurements; 2. Polarisation calibration; 3. Polarisation systematics removal (bandpass mismatch); and 4. Gain stability and noise properties.

In the LOEP we proposed an observational strategy based on "deep annuli", i.e., a scanning plan allowing for long integrations of a few selected narrow annular regions of the sky. The motivation for this choice was that, at the time of submission of the proposal, the extent of the 20-K cooler operation was highly uncertain, possibly leading to the acquisition of less than a full survey. The deep annuli concept was seen as a beneficial scanning strategy for a more limited and uncertain extension. A deep annuli scanning strategy would allow to align LFI and HFI sensitivity in the deep annuli regions (in addition to the polar caps, already deeply observed) to be used for cross-calibration and component separation. Furthermore, deep observations of bright HII regions were envisaged to be the best method to calibrate bandpass mismatch effect in LFI polarisation analysis. The deep annuli strategy would also improve the LFI observation of point sources, such as variable sources, quasars, polarised compact sources.

Since the submission of the LOEP proposal, three new factors have emerged which are relevant for the definition of the scanning strategy:

a) Detailed analysis has been carried out to assess the best scanning strategy for reaching the above mentioned objectives.

b) The ongoing *PLANCK* data analysis work has recently led to an increased interest in understanding low multipole power spectra ($l < 100$) both for breaking cosmological parameter degeneracies and for improving modelling of the Galactic foreground emissions and large scale magnetic fields (see Appendix A for further details). This has placed an even stronger emphasis on controlling polarisation systematics.

c) The "FM1" Sorption Cooler has shown excellent behaviour, largely outperforming the FM2 cooler, so that we are now confident that the *PLANCK* 20 K stage will last at least until June 2012 (see Appendix B), thus allowing at least one additional full sky survey.

In this report we summarise the investigations that we have performed in order to define an optimised scanning strategy for the LFI-only phase, taking into account all the available evidence, and we provide recommendations for its implementation.

2 Jackknife tests

At the time of writing the LOEP, the expected lifetime of the 20K stage based on extrapolation of the FM2 cooler performance was highly uncertain, and therefore we had to design a strategy which would be still useful in case of a short extended time. However, the excellent performance of the FM1 unit has reversed this situation. We are now confident that the *PLANCK* 20 K stage will be operational at least until June 2012 (Appendix B), and the most recent evaluation show significant margin over this date. Furthermore, we are also somewhat more optimistic that further observations may be permitted by regeneration of one of the Sorption Coolers at the end of this period, so although our detailed planning extends only until June 2012, we have allowed ourselves to contemplate observations of the key calibrators, Jupiter and the Crab nebula, in September 2012.

The now well established expectation to complete a sixth sky survey is a major driver for reconsidering the scanning strategy in view of the main objectives established in LOEP. In fact, by adopting a continuous sky coverage it would allow to perform a number of powerful differential tests, the so-called "jackknife", to improve diagnostics of systematic effects and calibration.

The "jackknife" is a statistical technique for estimating sample statistics using subsamples of data. This is a well-known procedure for cosmology experiments and has been applied in the analysis of numerous CMB experiments including BOOMERanG, QUAD and WMAP. For the LFI data analysis carried out so far, jackknife tests have proved extremely powerful for the identification of spurious signals, calibration analysis and self-consistency checks (Zacchei et al, 2011, Mennella et al, 2011). The significance of these tests is assessed with Monte-Carlo simulations. We have developed a number of different ways in which this method can be applied to the *PLANCK* data, as described in some detail in Appendix D.

A sixth survey will not only represent an additional element in the analysis, it will also provide a unique reference in the context of the overall *PLANCK* scanning strategy. The first four *PLANCK* surveys were carried out with the spin axis executing a 6-month period cycloid motion around the anti-Sun direction with a fixed phase $\phi_0 = 340°$ (see Appendix L for details). This choice allowed us to perform a number of powerful jackknife tests, e.g. between surveys 1–4 (sharing the same cycloid phase), and between surveys 1&3 and 2&4 (with identical patterns in the sky). In Survey 5, however, in order to improve our ability to remove high-frequency baselines and spurious polarisation signals, we shifted the cycloid phase to $\phi_0 = 250°$. While this shift proved successful for removing those effects, it left Survey 5 with a cycloid phase unmatched by other surveys. By maintaining in Survey 6 the same phase $\phi_0 = 250°$ as in Survey 5, we will have the possibility to perform jackknives between surveys 5&6, as well as 1–4 vs 5–6.

These tests are expected to be effective for obtaining the objectives indicated in the LOEP, i.e., polarisation effects, optical effects, and calibration. Comparison of surveys 5–6, and 1–4 will be a stringent test of our understanding of beam systematics, because of both the change of scan angle path between successive surveys and the change of phase for surveys 5 and 6. These survey-to-survey comparisons have been important in the past for validating improvements in the pointing model.

The analysis of spurious polarisation due to bandpass mismatch (the IQUSS condition numbers, discussed in the next section) shows that with the sixth survey we will be able to make systematics-cleaned single-horn frequency maps in polarisation, which enables a new class of jackknives. Not the least of these is that we

will be able to search for artefacts due to differential polarisation orientation errors between feed horns, providing a valuable cross-check on the orientation calibration from the Crab nebula (Section 6 below).

A general advantage of the sixth survey is to help distinguish periodic (e.g. annual) changes from secular changes over the mission lifetime. It may also be possible to distinguish multiplicative (i.e. calibration) from additive effects in the time streams, for example as a result of the sorption cooler switchover.

3 LFI bandpass correction for polarisation

Receiver bandpass mismatch is currently the most important source of polarisation systematic effects in the LFI. The principle effect is simply an effective frequency offset between the two polarisations, characterised by the so-called "*a*-factor", defined as

$$a = (\nu_s - \nu_m)/(2\nu_0),$$

where ν_0 is the receiver mean centre frequency and ν_s, ν_m represent centre frequencies of the main and side receiver arms which are differenced to provide the polarisation measurement. For an ideal receiver, the *a*-factor would of course be zero, and a non-zero *a*-factor controls the amount of leakage of temperature to polarisation, known as the 'spurious signal', $S = aL = a(\beta - \beta_{CMB})T^{\text{Foreground}}$, where β and β_{CMB} are spectral indices of the foreground and CMB (Leahy et al. 2010).

The spurious signal can be solved for along with the Stokes parameters at any pixel crossed by scans at several angles − indeed, this is how the *WMAP* team solve the problem. But for *PLANCK* this leads to large errors, since the range of scan angles is usually small. One of several possible improved correction schemes currently under investigation is the following three-stage process: (i) an initial, noisy, direct solution for *IQU* and the spurious signals in each *pair* of feed horns[1] (so-called *IQUSS* solution); (ii) a fit of these *S* maps to the leakage map *L* estimated from our foreground model, to determine the *a*-factors; (iii) subtraction of the model spurious signal, *aL*, from the data.

Current analyses based on nearly three surveys of data have determined the *a*-factors with statistical errors of typically 0.2%; but different estimators differ by up to 0.4–0.8% (see Fig. 1), where requirements for optimal polarisation recovery indicate that an accuracy of 0.1% should be attained.

Our current best results are from a Maximum Likelihood technique based on fitting the Large Magellanic Cloud Tarantula nebula, which lies in the multiply-scanned South Ecliptic pole region. In Section 4 below we show that the revised scanning strategy will achieve the 0.1% requirements for all the horns and also improve the *IQUSS* solutions across the sky, allowing for improved separation of systematics and signal.

[1] In the LFI focal plane, pairs of feed horns are aligned along the scan direction and each pair provides a self-consistent set of detectors to extract *IQU* parameters (the only exception is horn 24 at 44 GHz).

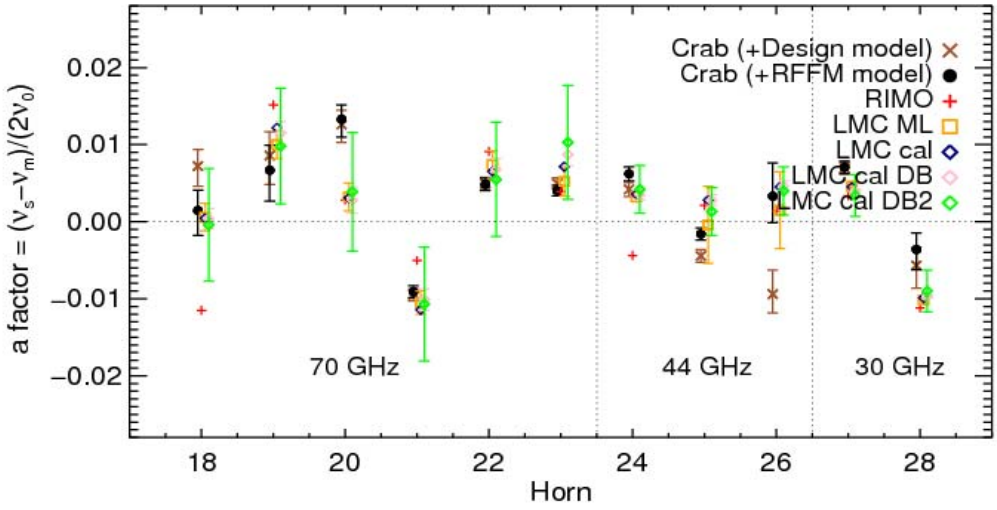

Fig. 1: The a-factors derived using nearly three surveys of data. Values from several different methods are plotted, showing the general agreement, with the LMC "Maximum Likelihood" ML method currently being favoured. The "RIMO" values are based on pre-launch measurements of the bandpass shape and are not expected to be accurate (see Leahy et al 2010).

4 Simulation of the sixth survey

The two scanning strategies considered in our studies are a smooth scanning law with the Survey 5 cycloid phase and a "deep ring" strategy, where a discrete number of rings in the sky are scanned deeply to increase sensitivity. In particular we focused on three different cases:

- Case 1: Surveys 1–5 (the reference case), which we also call NFS for "Nominal Five Surveys";
- Case 2: Surveys 1-5 + six additional months with the "Survey 5" cycloid mode (until July 12, 2012), which we call NFS+1;
- Case 3: Surveys 1-5 + six additional months with the deep annuli mode (until July 12, 2012), which we call NFS+DA.

The simulations were carried out by generating detector pointings for the different cases using "Level-S" software (Reinecke et al. 2006), and running "Madam" map-making software used for *PLANCK* processing. See Appendix C for further details.

Results for the 70 GHz channel are shown in Figs 2–4. For each case the three maps represent the hits map (top), the *IQU* (bottom left) and the *IQUSS* (bottom right) inverse condition numbers.

The condition number gives a measure of how much greater the noise variance on Stokes *Q* and *U* will be relative to the total intensity *I*, for a given scanning strategy (notice that we have plotted the inverse condition number). A condition number of 2 is the best-case scenario and will be larger in regions of sky where polarisation solutions are poorer.

Case 1

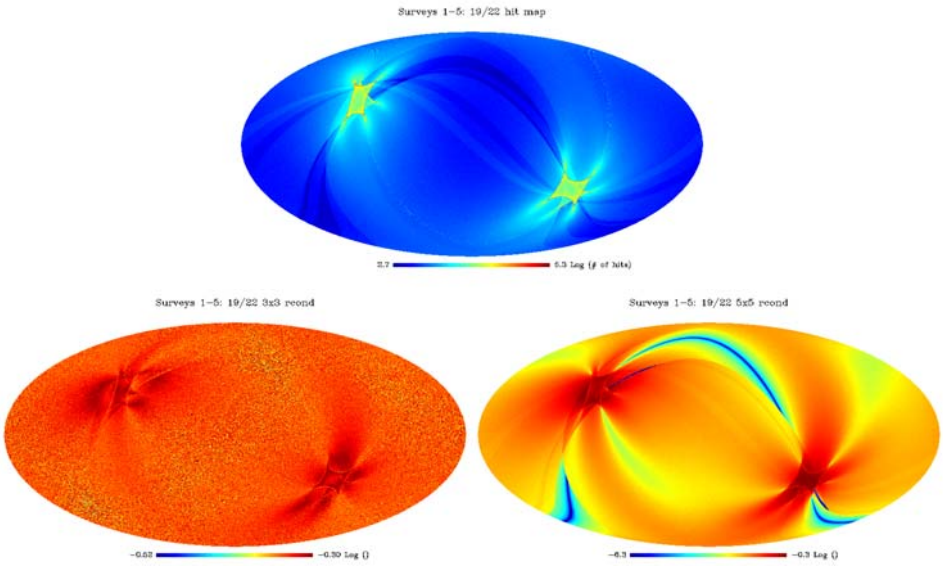

Fig. 2: The hits map (upper), the *IQU* inverse condition number (bottom left), and the *IQUSS* inverse condition number (bottom right) for the horn pair 19/22. Two of the degenerate longitude regions remain (very low *IQUSS* inverse condition number); the other two have already been eliminated by the changed scan path for Survey 5.

Case 2

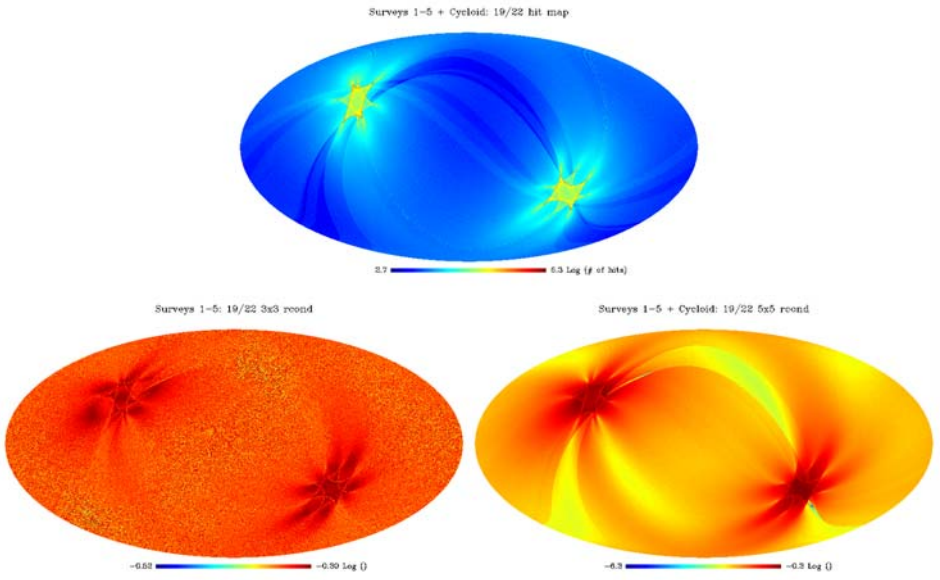

Fig. 3: The hits map (upper), the *IQU* inverse condition number (bottom left), and the *IQUSS* inverse condition number (bottom right) for the horn pair 19/22. The sixth survey improves the polarisation mapping in regions of sky which suffer from nearly parallel scanning (cf. *IQUSS* inverse condition number map in Fig. 2).

Differences in the effectiveness of the surveys can be seen in the IQUSS condition numbers. In Figures 2-4 it is shown that a smooth sixth survey significantly improves the map-making solutions in the regions of sky that up to now suffered from parallel scanning from survey to survey.

Case 3

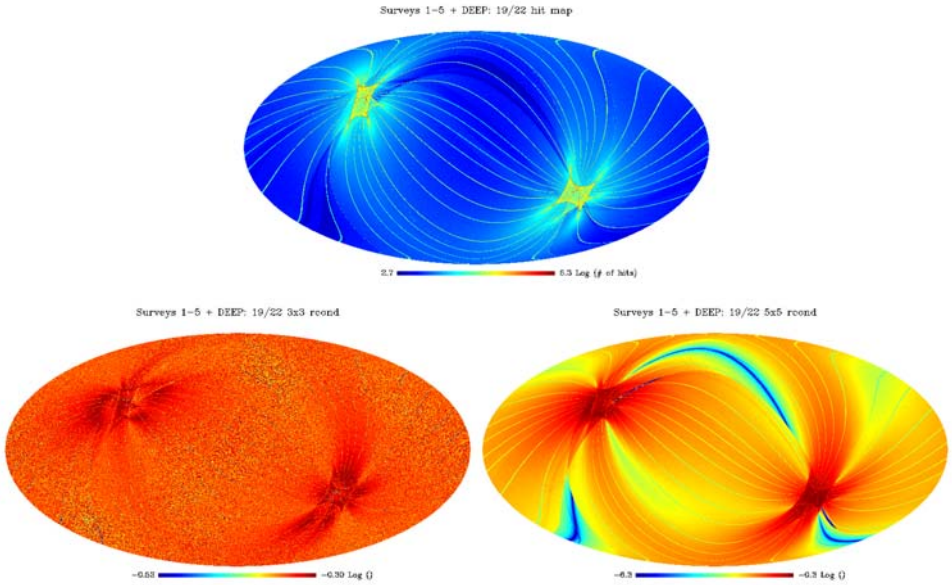

Fig. 4: The hits map (upper), the *IQU* inverse condition number (bottom left), and the *IQUSS* inverse condition number (bottom right) for the horn pair 19/22..

Our analysis based on both CMB and foreground shows that a requirement of 0.1% in the accuracy of the *a*-factor would ensure negligible impact of the bandpass effect. In Table 1 we show, for some representative LFI channels, simulations of the improvement in the accuracy of the *a*-factor determination provided by the sixth survey, assuming our preferred method of fitting to the Tarantula nebula.

Horn	(Case 1)	(Case 2)
19 (70 GHz)	0.0011	0.0010
22 (70 GHz)	0.0010	0.0009
25 (44 GHz)	0.0024	0.0007
26 (44 GHz)	0.0026	0.0008
27 (30 GHz)	0.00013	0.00012
28 (30 GHz)	0.00014	0.00012

Table 1: Forecasts for the a-factor error bars expected in Case 1 and Case 2 scanning strategies.

These results clearly show that a smooth sixth survey can reduce the error bars, especially for the 44 GHz horns LFI25 and LFI26. For these channels, in fact, a change in the scanning phase significantly increases

the spread in the scan crossing angles (see Appendix C), which is key for polarisation analysis. Moreover its location near the South Ecliptic Pole ensures that the observing time for the LMC is 3 to 6 times longer than the median (depending on the particular horn); thus we already have "deep scan" depth on this source. Note that in all cases we meet or surpass the 0.1% accuracy requirement. In the LOEP we quoted an expected precision of 0.5% using M42. It is possible that by optimising a deep annuli strategy over a number of bright HII regions (M42, Rosette Nebula, W3), one could also meet the 0.1% requirement – a possibility that we have not fully investigated, and for this reason we don't show a column for Case 3 in Table 1.

It should also be noted that the LMC will not be scanned by the LFI25 and 26 horns until June 30th. As a contingency in case of the unlikely event that the FM1 sorption cooler requires regeneration before this date, we are investigating two other options: (i) the LMC scan with these horns could be brought forward by modifying the scan strategy, at the cost of a sub-optimal scan orientation (ii) deep-annulus observations of a bright Galactic HII region at ecliptic latitude near -60 deg, (either Gum 29 or RCW38); this would permit three distinct scan angles with high-quality data. The trade-off to be made is between the better distribution of scan crossings for the LMC vs the higher signal-to-noise ratio for the Galactic nebulae (the mentioned HII regions are preferred to the ones suggested in the LOEP, for reasons of scheduling and potential scan geometry).

In conclusion, using the LMC with a continuous scan strategy we obtain excellent results for the correction of the bandpass effect without compromising the major benefits of a Survey 6 discussed in Section 2.

5 Beam reconstruction through Jupiter transits

Uncertainties in the beam knowledge will be a limiting factor for *PLANCK*'s scientific return. A 0.1% error in FWHM would imply a significant ~1% error in the window function, and therefore on the power spectrum, at multipoles ~1500 at 70 GHz, and at multipoles ~2000 at 100 GHz.

Using three "nominally scanned" Jupiter observations we have been able to measure the beams down to –25 dB at 70 GHz and down to –20 dB at 30 GHz and 44 GHz by averaging the measurements in square pixels of size 2 arcmin × 2 arcmin at 70 GHz and 4 arcmin × 4 arcmin at the other two frequencies. With these data we derived the main beam parameters (pointing direction, FWHM and ellipticity) from an elliptical Gaussian fit (Burigana et al. 2001, Zacchei et al. 2010). In Table 2 the typical statistical uncertainties in the FWHM determinations are reported.

	Single scan	Two scans	Three scans
70GHz	5" (0.6%)	4" (0.5%)	3" (0.4%)
44GHz	36" (2.0%)	26" (1.6%)	21" (1.3%)
30GHz	60" (3.0%)	47" (2.4%)	38" (2.0%)

Table 2: Uncertainties in the FWHM determination as derived from Gaussian elliptical fits of the beam maps derived from Jupiter measurements.

Jupiter measurements are also used to compare the beam maps with GRASP simulated beams. The 70 GHz channel is much more sensitive to variations, due to the shorter wavelength, although some differences may also appear at 30 and 44 GHz.

In 2012 Jupiter will be observable by *PLANCK* in two periods: around 16th January, at which point HFI may still be operating, and in September, which is only reachable if sorption cooler regeneration is successful.

A deep Jupiter scan by the LFI detectors will provide very useful data to discriminate among various telescope models. Furthermore, for the January 2012 observation, deep scans of Jupiter by the HFI detectors (if still operational) will be crucial for studying the bolometer time constant and sidelobes (see Appendix E). Several options are possible on how to distribute observation time through the beam profiles during Jupiter transit (e.g., uniform distribution across the beams, concentrate on one or few beam cuts). Our analysis shows that a full high signal-to-noise *UV*-plane scan through the LFI beams turns out to be very effective for recovery of optical parameters, and would also be adequate for the HFI observation. This plan has also the advantage of high operational simplicity, which is attractive given the possible HFI end-of-life occurrence. For the January 2012 observation, therefore, the baseline will be to scan the full *PLANCK UV*-plane with intensive sampling (0.5–1 arcmin repointing angle), as detailed in Appendix E. The precise U range will be optimised to maximize the sensitivity to plausible departures of the beam shape from our current model.

These measurements will also provide valuable data for planetary scientists, given *PLANCK*'s accurate absolute calibration. This in turn means that *PLANCK* measurements of Jupiter will provide the basis for the calibration of many future ground and space-based experiments operating at similar wavelengths. The proposed strategy for meeting this goal is to perform a nominal-like scanning with a scan step of ~0.5–1 arcmin in the cross-scan direction. Depending on the time available we can, for example, optimise the spacecraft movement in order to scan the beams at $U < 0$ (for LFI27, 28, 24, 18, 19, 20, 21, 22, 23) then move the satellite in order to point Jupiter towards the beams 25 and 26 ($U > 0$).

6 Crab Nebula

The Crab Nebula is the brightest polarised source at LFI frequencies, and hence is an obvious choice as an object to use for polarisation calibration. Deep-ring scans of the Crab Nebula during the extension can reduce the uncertainty in polarisation orientation of the worst-measured feed horns by a factor of two, bringing the error for all horns below 0.5°, comparable to *WMAP* (allowing for its systematic errors). This also enables the Crab to act as a check for the *a*-factor estimates of polarisation leakage. Detailed calculations of the improvement coming from deep scans of the Crab in March and September 2012 are presented in Appendix F.

A secondary benefit is that the Crab is an almost-unresolved and relatively isolated source (with a very well-measured fine-scale structure), which has a flux density much higher at LFI frequencies than any planet except Jupiter. Hence such deep ring observations can help constrain the beam pattern.

Finally, as with the Jupiter deep annuli, the deep scans will cut through various regions of low foreground signal where the improved sensitivity will allow locally exquisite very clean detection of the CMB polarisation, albeit along a narrow stripe which limits the precision of harmonic analysis (see Appendix G).

7 Power spectrum and low multipoles

Since this was another recommendation of the LOEP, we have also used an optimal angular power spectrum estimator to evaluate the benefits of the LFI extension at low multipoles. Results show a negligible

dependence of any improvement on the details of the scanning strategy. Further details are presented in Appendix H. The key issue for scanning choices is better knowledge of systematic effects, rather than the reducing of statistical noise. However, in principle, larger *IQUSS* condition numbers (see Section 4 and Appendix C), as in the case of the smooth option, could help other aspects of the cosmological data analysis. In general smooth scanning works better than deep annuli for the improved mapping of diffuse polarised foregrounds at large angular scales, and this is important for *PLANCK*'s primary cosmological goals.

8 Spin rate and H/K sampling

We have explored the possibility of increasing the spin rate of the satellite during the LFI-only phase, as this could, in principle, lead to a mitigation of the effects of *1/f* noise (Seiffert et al. 2002) on the LFI maps. Systems analysis shows that the spin rate could be increased to about 1.4 r.p.m. Telemetry margins are available after HFI is non-operational. While this is attractive in principle, the scientific benefit is not great and the risk factors (most notably those associated with the need to re-calibrate the REBA) lead us to not recommend this possibility. See Appendix I for a further discussion.

The LFI team is considering the possibility of increasing the sampling of some housekeeping (H/K) information (such as radiometer current monitoring) during the LFI-only phase, with no significant operational impact on the system.

9 The proposed scanning strategy

We now summarise the optimised scanning strategy that we are proposing:

- Jupiter scan in January 2012 in deep-scan mode, mapping all *PLANCK* beams, assuming that HFI continues to operate, and optimisation of LFI beams if only LFI operates (the latter point applies also to subsequent Jupiter transits, likely after SCS regeneration).
- Deep Crab scan in March 2012.
- For the remaining observations, continuation of the cycloidal scanning initiated in Survey 5.
- During the smooth survey parts of the LFI-only extension (outside the Jupiter and Crab deep rings), we will adapt the durations of the pointings so that most of the pointings lost during the deep rings can be recovered. This will ensure that Surveys 5−6 have reasonably complete sky coverage (although they cannot be fully complete).
- Deep scans on Jupiter and the Crab in September 2012, should sorption cooler regeneration prove successful.

  The following baseline is to be adopted for the January Jupiter scan:
  a. 27 Dec. – Jan. 8 : compressed pointings (2121 s) in order to recover 1.5 days worth of S5 pointings before the Jupiter deep scan (maximum recoverable).
  b. Jan. 8 – Jan. 15 : first part of Jupiter deep scan with HFI + LFI 25-26. Step size 1', 1550 seconds per pointing. This compression is necessary to allow HFI to have the whole focal plane scanned by Jupiter before likely end of life on January 15.
  c. Jan. 15 – Jan. 30 : second part of Jupiter deep scan with LFI main part. Step size 0.5', 3044 seconds per pointing.
  d. Jan. 31 – Feb. 6 : compressed pointings to 1903 s. This is to recover 3 days worth of S5 pointings (max. recoverable).

See Appendix F for the further analogous information on the Crab nebula.

10 The HFI support: 4-K cooler

During the LFI phase extension, the HFI IOT will continue to operate the HFI instrument and monitor a few house-keeping parameters to check the global health of the HFI electronic chain and the 4-K cooler behaviour. This task is expected to be executed by the MOC Spacecraft Controller, thus avoiding HFI or LFI IOT to be involved during DTCP. Should any anomaly be detected by the SpaCon, they will as soon as possible inform (by phone) the HFI IOT point of contact.

During the LFI-only phase it may be possible to adjust the 4K cooler as to obtain a slightly lower temperature of the 4K reference loads, which is beneficial to reduce the impact of 1/f noise in the LFI data. This possibility will be explored jointly by the HFI-LFI teams.

11 MOC support

MOC will continue to support the operations of the LFI-only phase in the same way as for the Routine Phase and the Mission Extension. The only foreseen change is in the duration of daily contact periods (known as DTCPs), which will reduce from 3 hours to 2 hours starting with the DTCP on 01/03/2012. This change reflects the reduced downlink time required to empty the on-board data stores once HFI is no longer accumulating science data.

12 Conclusions

According to the LOEP proposal, the main objective of the LFI-only extension of the *PLANCK* mission was to improve our knowledge of LFI systematic effects and calibration in order to optimise the science return of *PLANCK*. In particular, we identified four key instrument-related aspects: (i) optical beam measurements through Jupiter mapping; (ii) polarisation calibration and mapping of the Crab Nebula; (iii) effect on polarisation of the shape of the bandpasses; and (iv) gain stability and noise properties. After one more year of data analysis, we confirm that improved understanding of all of these remain as the main objectives of the LFI-only phase. Recent developments in the *PLANCK* data analysis have introduced an additional key point, i.e., the need to optimise low multipole power spectra analysis. However, further analysis has shown that deep rings would not definitely improve this issue either, and increased understanding of systematics is the prevailing principle for all aspects considered.

In this note we have discussed the optimal scanning strategy to achieve best results in the above points. The main conclusions are as follows.

1. Optical beam measurements

Detailed knowledge of the instruments beams and of the telescope optical parameters are key elements for the *PLANCK* data analysis. We confirm the high priority of deep observations of Jupiter to map *PLANCK* LFI beams. In January 2012 HFI is expected to still be operating. HFI has a strong interest in observing Jupiter to

study detector sidelobes and bolometer time constants. In this case, the LFI and HFI teams have agreed to scan the entire focal plane with ~0.5–1 arcmin re-pointing spacing.

2. Polarisation calibration

No changes with respect to the LOEP scan strategy are suggested. We confirm our intention to intensively scan through the Crab Nebula in order to reduce the uncertainty in polarisation orientation of the feed horns.

3. Bandpass effect on polarisation

Bandpass mismatch is the main systematic effect for LFI polarisation, including at low multipoles, and this in turn has an impact on the polarisation analysis of *PLANCK* as a whole. We performed detailed simulations to quantify the residual error in the leakage *a*-factors (which control the residual effect in the data) focusing on the LFI-only phase. The proposed "smooth scan" strategy is able to achieve the desired error reduction, up to a factor of 3 for the 44 GHz channels. The important factor in the improved recovery is the *scanning of the LMC over a large set of scanning angles*.

4. Gain stability and noise properties

No changes with respect to the LOEP scan strategy are suggested. The determination of an accurate gain model is essential for LFI data analysis. The radiometer gain and noise properties are independent of the details of the scanning strategy, but smooth scanning allow jackknife tests to be performed with previous surveys, highlighting gain variation effects, particularly those due to thermal conditions of the FM1 cooler close to its end-of-life.

5. Jackknife tests

Smooth scanning is much more effective than deep annuli if an extra full-sky can be completed. We now have evidence that a sixth survey can be completed thanks to the excellent performance of FM1 20K cooler. A new full-sky map, with the phase shifted scheme, will allow for a number of powerful differential checks, particularly jackknife tests, which have proved highly valuable in highlighting residual systematic effects, particularly at low multipoles.

6. Deep annuli for ancillary science

The original LOEP emphasised the utility of deep annuli for two ancillary science programmes, Galactic and extragalactic foreground separation, and studies of extragalactic radio sources. The deep annuli greatly increase the LFI sensitivity in restricted regions and hence at small angular scales, and the annuli planned for Jupiter and Crab observations will also be exploited for these purposes. However, these programmes are lower priority than the need to improve the LFI calibration, and the largest revision in the scan strategy is the elimination of deep rings targeted on ancillary science in favour of smooth scanning. This allows the whole sky to be mapped for an additional one (perhaps even two) surveys, resulting in a benefit for characterising diffuse foregrounds at large angular scales, and will accumulate two further sets of measurements for *all* sources, with a significant impact for long term variability studies.

In conclusion, our recommendations for the scanning strategy during the LFI-only phase are the following:

- **Continue with the scanning strategy of Survey 5 for the rest of the observing time;**
- **Confirm deep scans through Jupiter and Crab Nebula;**
- **Maintain the 1 r.p.m. spin rate.**

Appendix A: Polarisation at large angular scales

An important scientific goal of the *PLANCK* mission is the mapping of the sky in polarisation at low and intermediate multipoles ($l \leq 100$), corresponding to angular scales larger than 1–2 degrees. Polarisation at low multipoles provides accurate extraction of polarised and cross-correlation modes of the CMB angular power spectrum, which are critical for breaking degeneracy in cosmological parameters estimation. In addition, it provides important data for a detailed understanding of Galactic foreground emission and large-scale magnetic fields. The role of LFI is crucial, in particular, for the study of polarised synchrotron emission, the accurate modelling and removal of which will benefit the whole *PLANCK* analysis. At frequencies in the LFI range, 30–70 GHz, the Galactic foreground is low at large scales and, in particular, the LFI channel at 70 GHz falls in the minimum of large-scale polarised foregrounds. This aspect is unique to *PLANCK*, even in the light of recent ground-based experiments, such as ACT and SPT, that are contributing to the study of the CMB anisotropies at high multipoles. Furthermore, the high-resolution all-sky HFI maps will have much lower noise than any other experiment at multipoles up to few thousands.

It is well known that polarisation systematic effects at low multipoles are particularly difficult to track. Therefore, given the current status of the *PLANCK* data analysis at low l, there is a renewed focus on optimising the LFI-only survey towards large-scale polarisation information. In the previous study of the LFI-only extension, we focussed on the deep annuli option, as a reasonable observational strategy for optimising our understanding of systematic effects. Assuming white noise only, one expects no significant difference in terms of recovered spectral information between the deep annuli and smooth scan approaches. We have verified this in detail (see Appendix H). On the other hand, large scale features in the sky directly are only observed with observational strategies that cover the whole sky more uniformly.

In Fig. A1 we summarise the sensitivity to CMB polarised modes for the *PLANCK* mission until the end of the 0.1-K dilution cooler lifetime. We show the case of instrumental noise only (black dots) and the case of noise plus cosmic and sampling variance (green dots and dashes, respectively, for the B-modes and the E-modes). For comparison, we also show various estimates of Galactic foregrounds at 70 GHz (red lines), with and without removal (see caption for details). Similarly, we show the expected contribution from extragalactic sources with and without removal (green lines), and the contribution due to lensing (blue dots). Clearly, the possibility of achieving low values of tensor-to-scalar ratios relies on the quality of the overall *PLANCK* data analysis.

The LFI data will improve over *WMAP*, thanks to a sensitivity better by a factor ~3 on the same reference pixel and frequency (and a factor ~2 even for the highest frequency comparison of *WMAP* vs LFI), i.e., about one order of magnitude in the angular power spectrum. In principle, this allows LFI to probe the low-multiple bump of the B-modes power spectrum for tensor-to-scalar ratios of ~0.03–0.1, and to contribute to a significantly better understanding of the synchrotron polarised foreground at large angular scales. This largely relies on accurate understanding and removal systematic effects using an optimal analysis of the data. The smooth scan strategy allows us to directly probe large-scale information with a sixth survey, which gives additional tests of systematic effects at large angles (see previous sections), and it is therefore advantageous for large scale science.

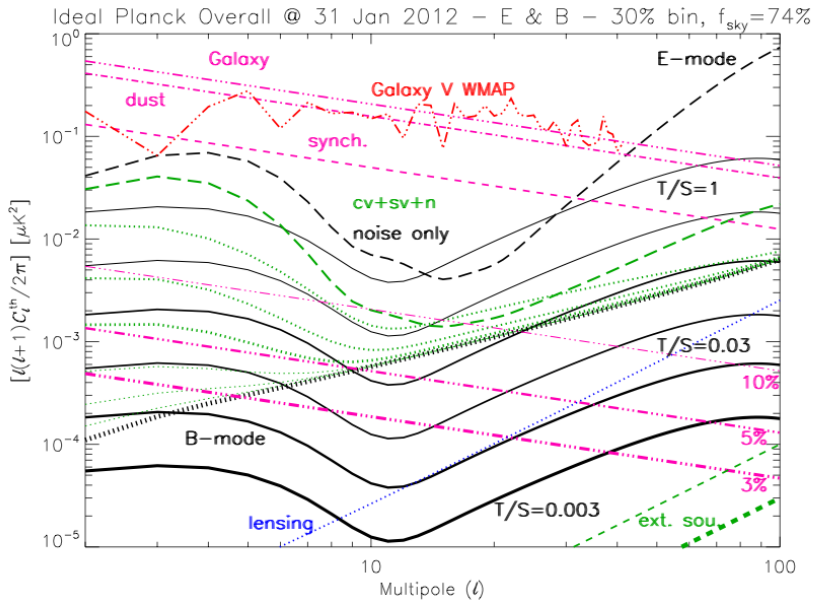

Fig. A1: CMB E polarisation modes (black long dashes) compatible with *WMAP* data and CMB B polarisation modes (black solid lines) for different tensor-to-scalar ratios *T/S*=*r* of primordial perturbations) are compared to *PLANCK* overall sensitivity to the power spectrum for the whole mission, assuming the noise expectation has been subtracted. The plots include cosmic and sampling variance plus instrumental noise (green dots for B modes, green long dashes for E modes, labelled with cv+sv+n; black thick dots, noise only) assuming a multipole binning of 30%. Note that the cosmic and sampling (74% sky coverage excluding the sky regions mostly affected by Galactic emission) variance implies a dependence of the overall sensitivity on *r* at low multipoles, relevant to the parameter estimation; instrumental noise only determines the capability of detecting the B mode. The B mode induced by lensing (blue dots) is also shown. Galactic synchrotron (purple dashes) and dust (purple dot-dashes) polarised emission produces the overall Galactic foreground (purple three dot-dashes). *WMAP* 3-year power-law fits for uncorrelated dust and synchrotron have been used (Page et al. 2007). For comparison, *WMAP* 3-year results (http://lambda.gsfc.nasa.gov/) derived from the foreground maps using HEALPix (Gòrsky et al. 2005) tools (available at http://healpix.jpl.nasa.gov/) are shown: power-law fits provide (generous) upper limits to the power at low multipoles. Residual contamination levels by Galactic foregrounds (purple three dot-dashes) are shown for 10%, 5%, and 3% of the map level, at increasing thickness. We plot also as thick and thin green dashes realistic estimates of the residual contribution of un-subtracted extragalactic sources, $C_l^{res,PS}$, and the corresponding uncertainty of sources, $\delta C_l^{res,PS}$

Appendix B: Prospects for cooler lifetime and possible regeneration

The two *PLANCK* Sorption Coolers ("FM1" and "FM2") have been designed to meet their performance requirements (about 1 W of cooling with 470 W of input power) for a total of two years, which includes 18 months of flight and 6 months of ground testing. The FM2 unit was operated from June 2009 until August 2010 when the system started to show accelerated degradation. On 11th August 2010 the switchover operation activated the FM1 unit. The analysis following the unexpected behaviour of the FM2 concluded that with a new operational strategy the FM1 could last until the end of the HFI dilution, foreseen for January 2012.

There are two main issues relevant for cooler degradation: (i) Hydride degradation as a function of the number of cooler cycles; (ii) Gas-gap degradation due to H_2 permeation. The first issue is controlled by

progressively increasing input power during the mission, up to the maximum power available from the Spacecraft to a single bed (250 W). This limit is considered as the system end-of-life (EOL).

The hydrogen gas permeation is strongly dependent on the temperature of the bed. To minimise its contribution, the final desorption temperature of the compressor element has to be kept as low as possible. This is achieved by progressively decreasing (compatibly with the input power increase) the cycle-time.

The degradation effects can be reversed by subjecting the hydride alloy to elevated temperatures under reduced pressures (relative to chemical equilibrium); this process is known as "regeneration", and can be run in-flight to restore hydride sorbent capacity up to about 90%. Regeneration operation requires stopping the cooler cycle, so the LFI temperature passively rises up to the VG3 value and scientific observations must be suspended. The system is sent by tele-command into Regeneration Mode where power is provided to Bed 1 to let it slowly desorb its H_2 gas content down to the minimum pressure that can be maintained by the hydrides capacity. Once this minimum pressure is reached the bed is heated up to around 670 K for 4 hours. At that point the bed is allowed to cool down to the radiator temperature and the same procedure is applied in sequence to all other 5 beds. The whole operation takes about 4–7 days mainly depending on the time needed by each bed to reach the minimum pressure. The cooling chain can then be restarted and cool-down is completed in about another week. The performances of the regenerated cooler are immediately monitored to assess the potential extended life recovered. In total the full process requires suspension of LFI scientific observations for about round 2 weeks.

Unfortunately, regeneration has a negative impact on gas-gap contamination and can degrade their expected life time. In addition, the loss of capacity in the two coolers will result in the regeneration process occurring at higher pressures than previously tested. At this point it is not known what the resultant recovery will be under these conditions.

At the time of writing, the performance of the FM1 cooler, in terms of both the input power and final desorption temperatures, is exceeding that of the FM2 cooler and the JPL tests. This has allowed for an extension to the estimation of EOL for the *PLANCK* Sorption Cooler.

According to the latest estimates (Pearson 2011), the gas-gap lifetime is expected to be longer than the hydride lifetime. FM1 hydride life projections, based on current performance, should allow us to reach June 2012, while the gas-gap lifetime is now estimated to reach August 2012. This means that at the end of FM1 operations (June 2012) a regeneration procedure may be attempted without impacting the baseline LFI-only phase. This process might yield an additional 3–6 months of lifetime. Approximately one month more is still available in the off-state cooler (FM2). This FM2 life is considered as an extra margin, since the cooler will be run in “degraded operations.”

Appendix C: Simulations

We have carried out detailed simulation to evaluate the condition number (see Section 4) and covariance matrices for different scanning strategies. The detector pointings were calculated as follows. We first run a Level-S code, called *simmission4*, to produce a file that contains pointing information according to a scanning strategy, and dynamical parameters of the satellite. For the dynamical parameters we used values presented in the Level-S manual (Reinecke et al. 2006). Using the pointing information file and *multimod* (again, part of Level-S) we reconstructed the detector pointings of the satellite as a function of time. For pointing reconstruction and instrument noise, we used the most up-to-date instrument database (associated with the data exchange DX7).

Using the Madam map-making software and additional analysis tools (Keihänen et al. 2004) we calculated for each scanning strategy: hit maps, white-noise covariance matrices, low resolution full covariance matrices, and Stokes *IQU* and *IQUSS* “condition number” maps which give a measure of the quality and uniformity of the polarisation measurements.

The low resolution noise covariance matrices were calculated per LFI frequency channel, while the other products were calculated for a representative set of LFI horn pairs (i.e., aligned in the scan direction), namely 27/28 at 30 GHz, 25/26 at 44 GHz, and 19/22 at 70 GHz. These three pairs cover the geometrical extremes of the focal plane.

These simulations provided the hit maps, *IQU* condition numbers and *IQUSS* condition numbers shown in Section 4. The latter clearly favour a smooth scan strategy. Fig. C1 shows details of the hits map around the LMC (Tarantula nebula) from LFI 25/26. The SEP deep region shrinks to two almost disconnected triangles for these horns and hence the Tarantula is outside its border. But Survey 6 scans it in a new direction, giving the large reduction in *a*-factor errors noted in Section 4.

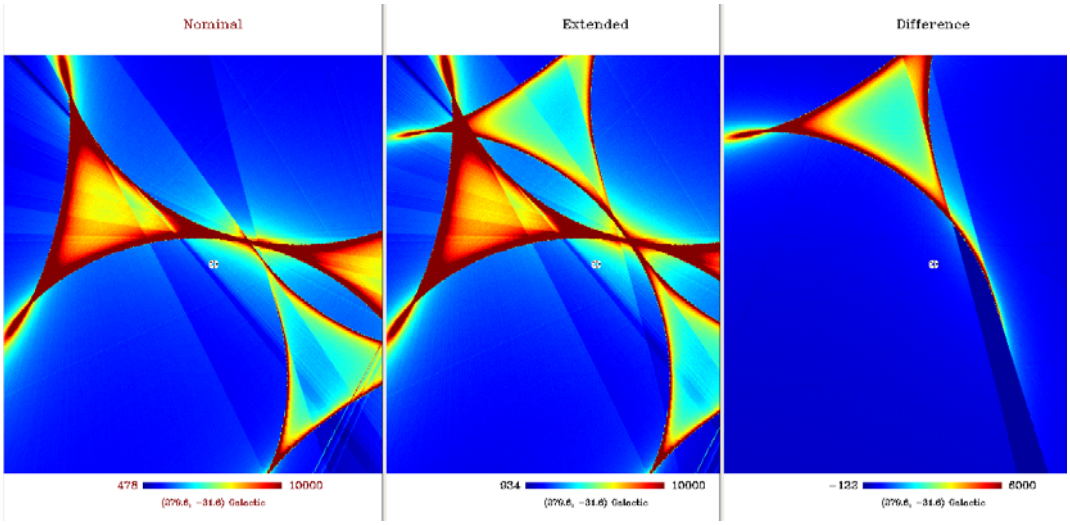

Fig. C1: Hits map for the 44 GHz horns LFI25/26 near the LMC. Note that it is close to the '44 GHz cusps' in the scanning strategy. Left: NFS; middle: NFS+1; Right: Survey 6 only.

Figs. C2–C7 show plots of *IQU* covariance matrices for sample LFI detectors. No relevant differences between the different strategies can be inferred from these results (though of course the covariances for *Q, U* and the spurious signals in the *IQUSS* solutions are dramatically reduced, as indicated by the change in the condition numbers).

Case 1: Surveys 1–5 (“Nominal Five Surveys”, NFS)

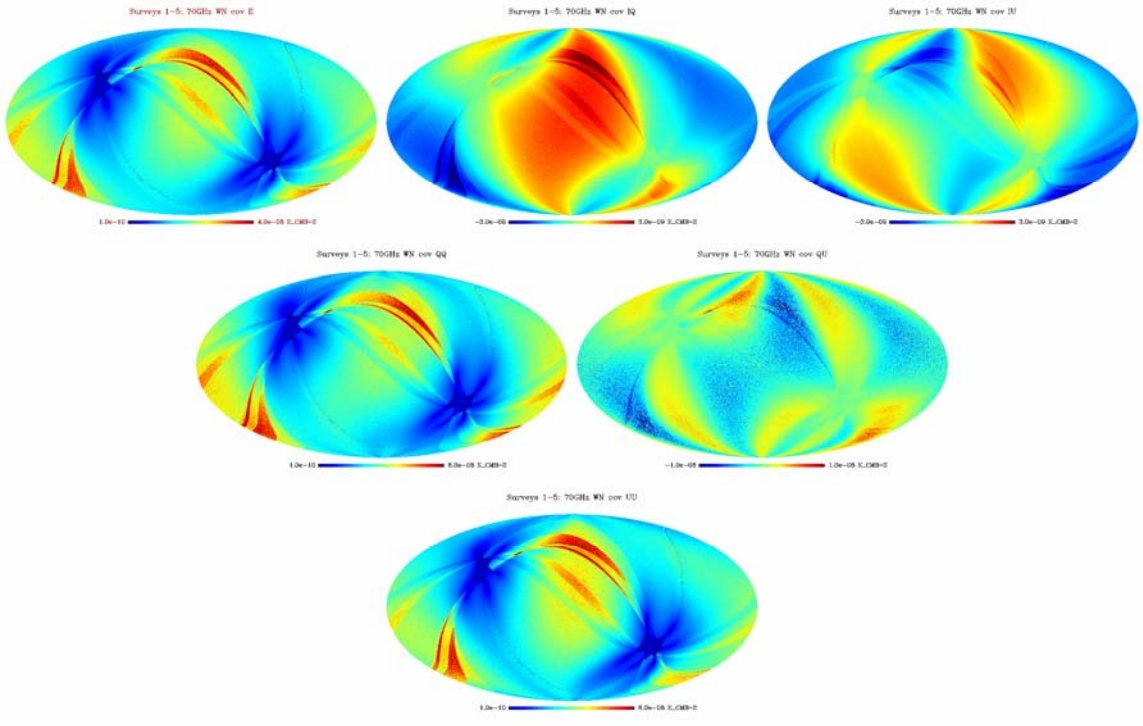

Fig. C2: The white noise covariance matrix elements for LFI horn pair 19/22 (70GHz). Top row (left to right): *II*, *IQ*, and *IU*. Middle row: *QQ* and *QU*. Bottom: *UU*.

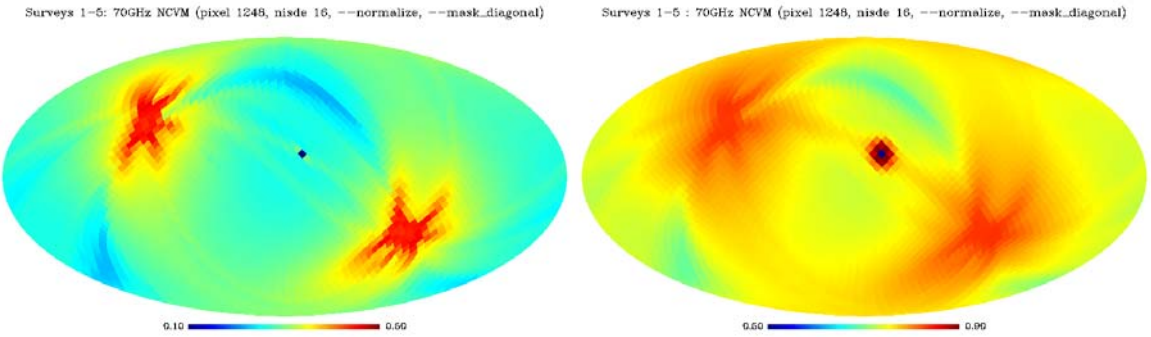

Fig. C3: The *TT*-covariance for reference pixel 1248 for the 70GHz frequency channel. On the left-hand side is the unsmoothed matrix, while on the right-hand side is the smoothed matrix (beam FWHM of 440 arcmin).

Case 2: Surveys 1–5 + six additional months in "Survey 5" cycloid mode

- **until July 12, 2012 (NFS+1)**

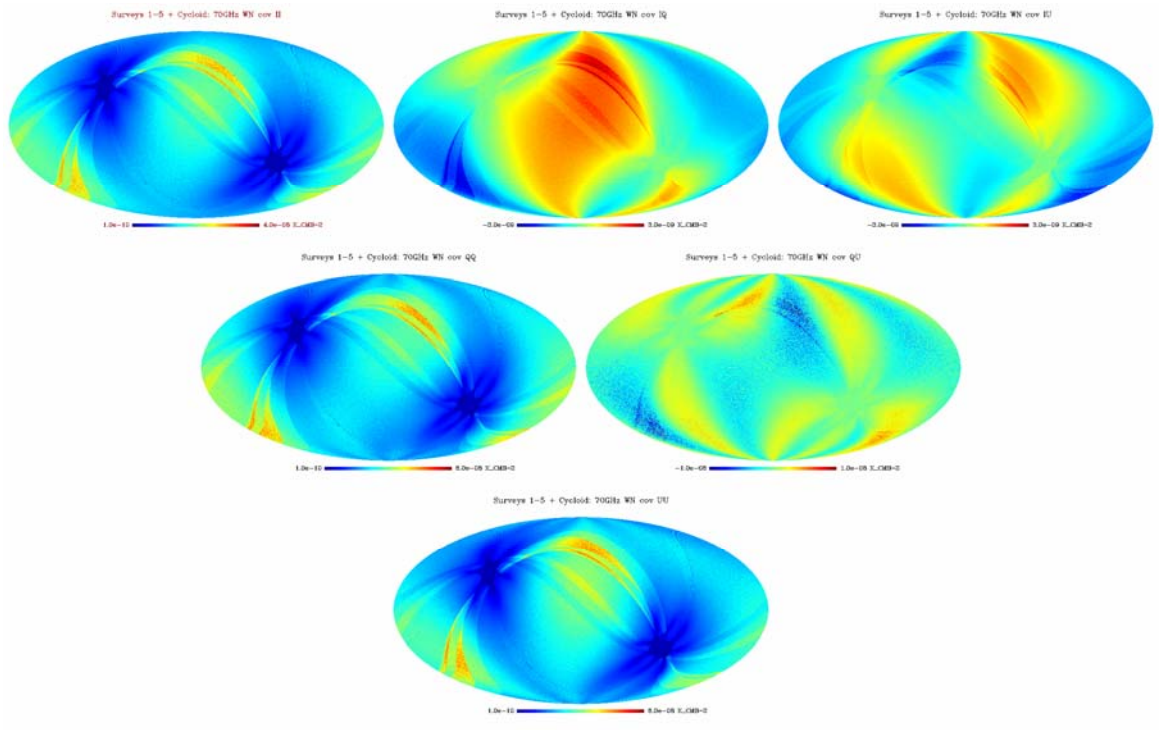

Fig. C4: The white noise covariance matrix elements for LFI horn pair 19/22 (70GHz). Top row (left to right): *II*, *IQ*, and *IU*. Middle row: *QQ* and *QU*. Bottom: *UU*.

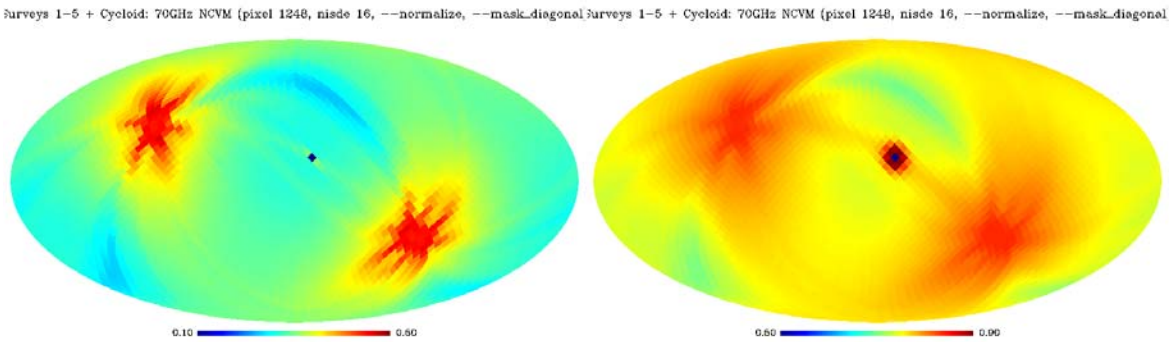

Fig. C5: The *TT*-covariance for the reference pixel 1248 for the 70GHz frequency channel. On the left-hand side is unsmoothed matrix, while on the right-hand side is the smoothed matrix (beam FHM of 440 arcmin).

- **Case 3: Surveys 1-5 + six additional months in "deep annuli" mode,**
- **until July 12, 2012 (NFS+DA)**

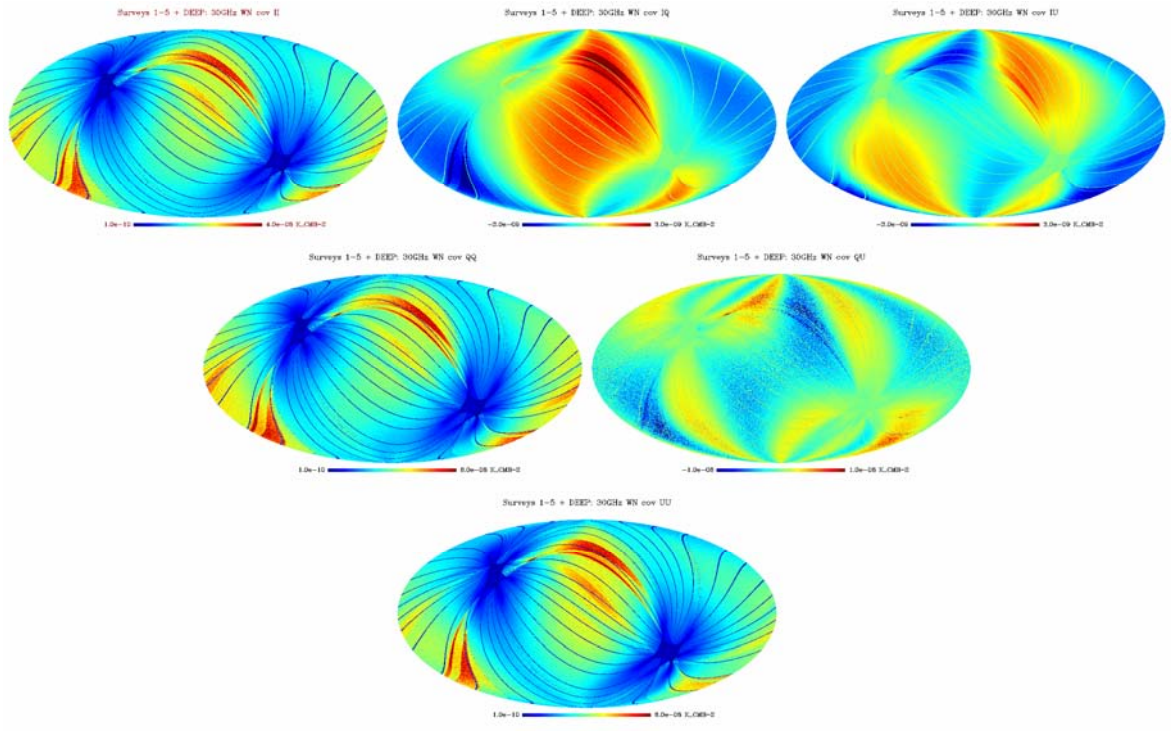

Fig. C6: The white noise covariance matrix elements for LFI horn pair 19/22 (70GHz). Top row (left to right): *II*, *IQ*, and *IU*. Middle row: *QQ* and *QU*. Bottom: *UU*.

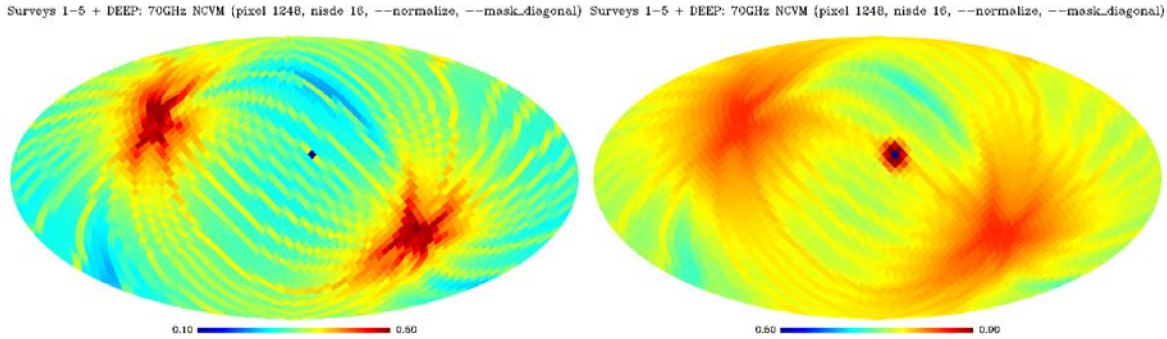

Fig. C7: The *TT*-covariance for the reference pixel 1248 for the 70GHz frequency channel. On the left-hand side is the unsmoothed matrix, while on the right-hand side is the smoothed matrix (beam FWHM of 440 arcmin).

Appendix D: Jackknife method as a tool to investigate systematic effects

Here we outline some of the main implementations of jackknife tests that will be applicable to the LFI data set by carrying out the LFI-only phase with a continuous scanning strategy.

D.1 Survey-to-survey jackknife

Each *PLANCK* survey lasts around six months. By comparing data from different surveys at both the map and power spectrum level we can assess the presence of long term calibration drifts, and then correct for its effect. In this respect, the sixth sky survey will extend the timescale over which we can assess the stability of the instrument, and therefore will improve our ability in disentangle multiplicative and additive effects.

Moreover, surveys 1 and 3 share the sky coverage and beam orientation, and the same applies to survey 2 and 4. Hence, we expect that in the absence of systematics, the difference map between survey 1 and 3 (likewise for the survey 2 and 4 difference) contains only instrumental noise. By computing the cross-power spectrum between these two difference maps we can assess and quantify the absence of residual signals. Also, owing to the change in phase of the scanning strategy cycloid phase from survey 5 onwards, comparison of the survey 1–2 difference with the difference between 5–6 will also be a powerful way of identifying any beam-related residual systematic effects.

D.2 Channel-to-channel jackknife

LFI 70 GHz horns can be pair-wise combined to obtain three independent temperature and polarisation maps which we usually refer to as quadruplet maps. Due to the geometry of the focal plane, the best combination is LFI18/23, LFI19/22 , and LFI20/21. These maps can be combined in many different ways to check for the presence of systematic effects: for instance one can compute the difference between maps from LFI18/23 and from LFI19/22, and build the temperature and polarisation cross-spectra with the third map LFI20/21. In the absence of systematics this is expected to contain no signal. However, at the current status this consistency test is affected by the presence of spurious signals mainly due to bandpass mismatch. As shown before, the presence of a sixth survey will improve the map-making solution for a 5×5 *IQUSS* systematics-removed horn-pair map in the region with parallel scans, thus allowing for a more stringent consistency check.

D.3 First/second half ring jackknife

Each pointing period last about 45 minutes, during which each *PLANCK* horn scans a ring on the sky at 1 r.p.m. speed, thereby performing about 45 circles. After removing the initial part where the pointing is unstable, typically 4–5 minutes, the remaining data of the pointing period consist of about 40 scans of the same circle on the sky that can be split into two halves to produce two individual maps. These maps contain the same sky signal as they share the same scanning strategy. However, the actual noise in the two maps will differ as they are built with different time ordered data samples, although the noise properties will be consistent. Hence, in absence of systematic effects, by taking the difference of the two half-ring maps for a given horn we obtain a noise-only map representative of the noise properties of that detector. By comparing the results from different sky survey we can estimate variations in the noise properties of the detectors in an independent way with respect to the “official” noise estimation pipeline. Adding a sixth survey will extend our capability in distinguish between long term and periodic variations and will also allow us to make half-ring jackknife polarisation maps.

Appendix E: Beam reconstruction through Jupiter transits

For the LFI instrument, Jupiter is by far the best source to obtain direct information on main beam shape and detector pointing properties. In this Appendix we discuss the criteria and baseline approach to optimise the integration time on Jupiter (Section E.1); the HFI requirements on Jupiter observations (Section E.2); and the baseline implementation of the Jupiter observation (Section E.2), depending on whether or not HFI will be operational in January 2012.

E.1 Criteria for Jupiter transit observations

During Jupiter transit, the scanning strategy can be arranged to distribute the detectors integration time in different ways (e.g., a uniform full-sky intensive observation of the entire focal plane, a few deep cuts through some of the beams, etc). This appendix reports some considerations useful for a comparison between different options based on a χ^2 analysis.

We focus on the ability of the observations to distinguish between two different beam models (RFFM and RFFM-SV) at 70GHz for horn LFI 18. The two beam models are displayed in the left panel of Fig. E1. In the right panel, we overplot the two beams after applying a shift on the beam centre of the RFFM-SV model to make the two beam centres coincident (within the available resolution of beam tabulation).

The ratio between the two models (or their relative difference) does not change much in the beam *UV* plane (see Fig. E2), but this does not imply that different beam regions are equivalent in terms of their contribution to constrain optical models. This is evident when comparing the signal produced by Jupiter observed at different positions in the *UV* plane for the two optical models: it ranges from $\approx 10^4$ μK close to the beam centre to ≈1μK at the edges of the beam *UV* region considered (see Fig. E3).

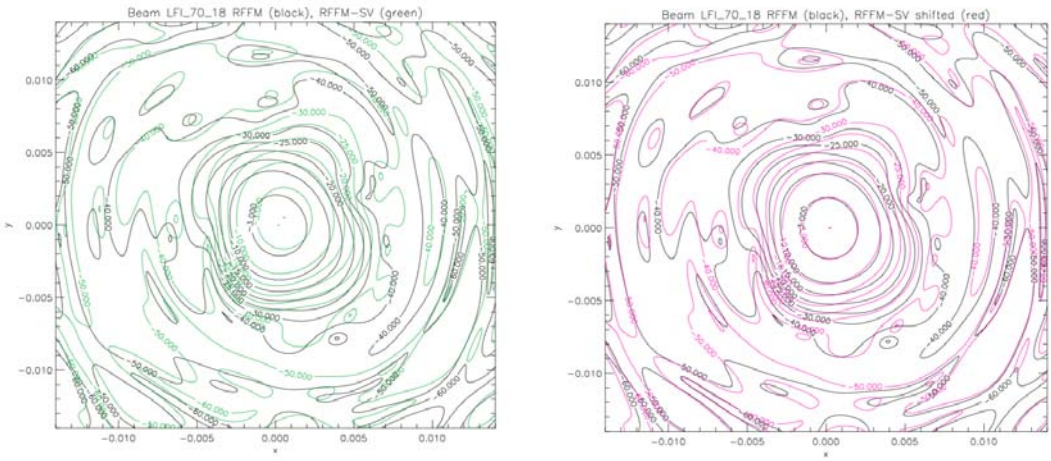

Fig. E1: Left panel: beam contour plots (in dB) for the two beam models considered (normalised to 1 at the maximum). Right panel: as in the left panel, but with the beam RFFM-SV shifted to have its centre in the same direction of RFFM (within the beam tabulation accuracy).

Let us assume that one of the two models represents the true beam, and (of course) the other does not. Assuming the typical LFI sensitivity and sampling time (Bersanelli et al. 2010, Mandolesi et al. 2010), we can compute the contribution to the χ^2 of each data sample as function of its position on the beam *UV* plane (Fig. E4). As shown, the ~4 orders of magnitude in signal ratio translates into ~8 order of magnitude in the χ^2 contribution ratio passing from the inner to the outer regions of the main beam.

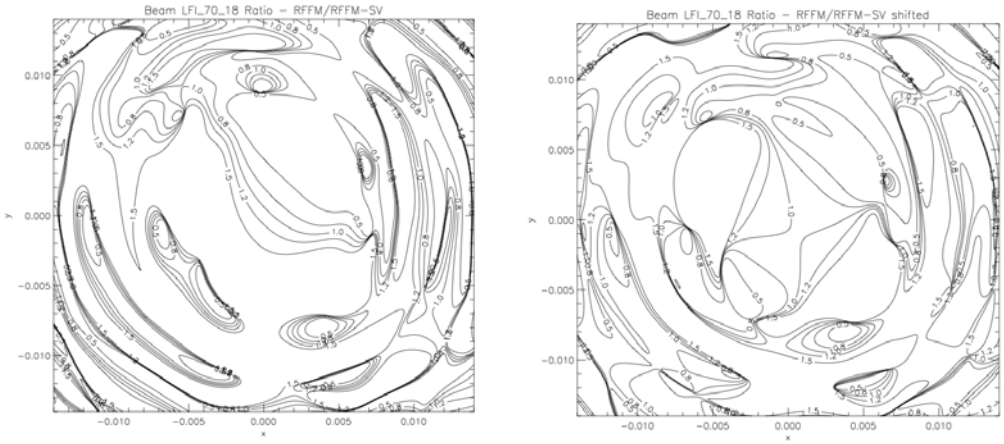

Fig. E2: Left and right panels: ratio between the beam response (on a linear scale), for the cases reported in the titles.

Using these plots we can compare the ability to achieve beam reconstruction for different scanning strategies. For example, for a typical 70 GHz beam, comparing the standard *PLANCK* scanning strategy (the one applied in previous Jupiter transits) with a deep 6-day mapping with 0.5 arcmin repointings (which we call "intensive mapping") we get an improvement of a factor ~2.5 in the beam parameter recovery.

In the case of a single deep cut at a fixed angle (or a few cuts) the global χ^2 will depend of course on the location of the beam cut with respect to the detector beam. One could expect that by concentrating the observation time near the beam centre, the χ^2 test would be more sensitive than in the case of the "intensive mapping" case (although not by a large factor). A detailed computation for the examples considered here suggests that this statement is highly model dependent. In fact, we find that the average of the contributions to χ^2 is: *(i)* 4.46, or 0.190 if we apply the beam shift, considering the whole available field (see Fig. E4); *(ii)* 24.6 (24.8), or 0.13 (0.15) if we apply the beam shift, considering only a single cut (five cuts) passing through the beam centre (or one cut through the beam centre plus the four cuts closest to it according to the available beam tabulation). This indicates that one (or few) very deep cut(s) could be more advantageous but only under some particular assumptions (in the considered example, if we compare beams that mainly differ in their centre positions) while "intensive mapping" is less model dependent, more robust and advantageous to compare beams that differ in shape. Furthermore, the "intensive mapping" case has three advantages over the single dip cut:

a) It directly maps the full beam, so that it allows to draw more model independent conclusions on the beam shape than those based only on a single cut.

b) It is optimal not only for the recovery of beam shapes, but also of focal plane geometry through precision measurements of relative positions of the beam centre directions. A few deep cuts through the focal plane, instead, would provide a less direct information. This analysis is quite important to study long-term drifts in the *PLANCK* optical system, which the LFI-only phase well is suited for.

c) For the January 2012 Jupiter transit, the need for HFI to also observe Jupiter and the possible coincidence with HFI end-of-life strongly suggest a operationally simple scanning strategy.

In conclusion, for the 2012 Jupiter transit we propose to adopt an "intensive mapping" scheme, as specified in Sect. 6, to be possibly optimized in the future[2] on the basis of precise definition of the optical models to be compared, the overall location of beams and the above items.

[2] For the considered beams we find for example that the average of the contributions to χ^2 is 26.5, 17.4, 11.7 (or 0.82, 0.73, 0.50 if we apply the beam shift) when we consider the scans at within distances from the beam centre of 1, 2 or 3 FWHM/2.

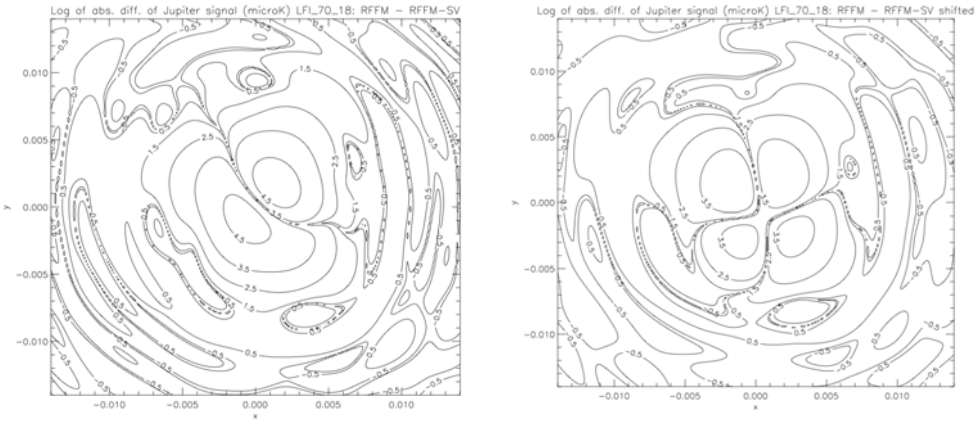

Fig. E3: Contour plots of the absolute difference of the signal (on a log scale) produced by Jupiter, assumed to be observed with one beam or the other beam, for the cases reported in the titles. A representative Jupiter peak signal of 280 mK (at 70 GHz) is assumed.

E.2 HFI requirements

Jupiter saturates the HFI main beam, and due to extended time constants, the data immediately following transit through the main beam are also corrupted. But scans adjacent to Jupiter transits are useful to map the beam pattern relatively far from the beam centres (i.e. the so-called "near far-sidelobes"). This helps both in the fine recovery of optical properties (and thus the removal of related systematic effects) and in the reconstruction of the instrument transfer function.

Note that in the case of HFI beams, it is important that rings in the telescope field of view crossed by Jupiter are not too close to the main beam centres but lie at angular distances ~0.5°–1°. Also, in order to achieve the necessary sensitivity, the HFI team requires about 4–6 days of integration to be spent mapping the field of view region relevant for HFI detectors.

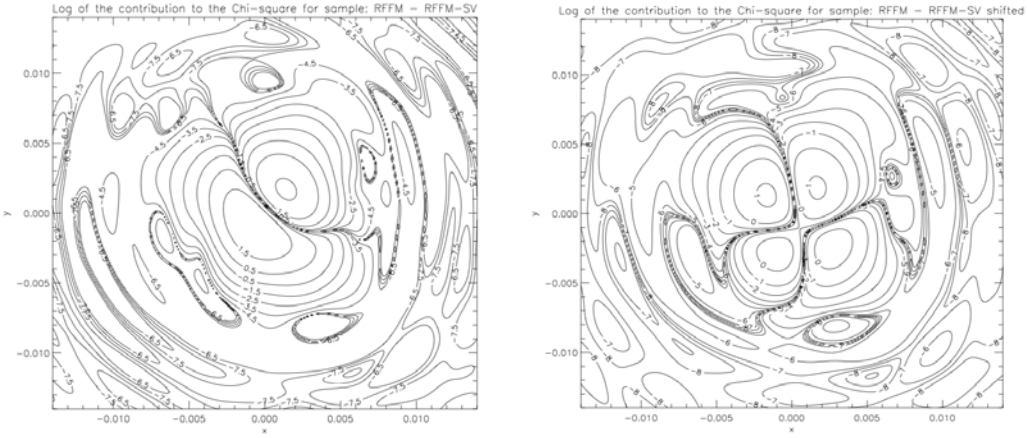

Fig. E4: Contour plot of the contribution to the $\chi 2$ (on a log scale) from each data sample, when one assumes that the true beam is one of the two, but the assumed model is the other one, for the cases reported in the titles. Sensitivity (μK×sec1/2) are those reported in the LFI pre-launch papers, and sampling time corresponding to 4 arcmin on the sky. The average of the contributions to $\chi 2$ over the whole available field is 4.46, or 0.190 if we apply the beam shift.

Fig. 5 shows the *PLANCK* field of view (see Tauber et al. 2010b for more details). Note that the *V* direction is essentially parallel to the scan for specific rings on the sky, while the *U* direction is covered as the spacecraft

spin is re-pointed. The beams are sufficiently densely packed that scans through the focal plane measure the pattern of several of them at once.

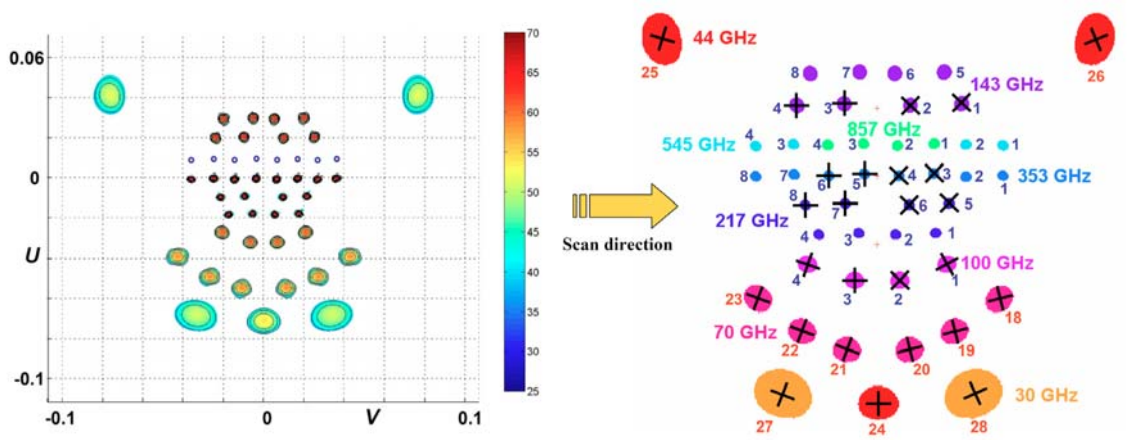

Fig. 5: The *PLANCK* field of view with beam contour plots (left panel) at the different frequencies (right panel). From Tauber et al. 2010b.

E.3 Mapping beams

Case A: Both LFI and HFI are operational

Assuming that in January 2012 both LFI and HFI will continue to operate, we propose to map the whole relevant region of the *UV* plane with equal spacing along the *U* direction in the *U* range: [−0.09, 0.06], corresponding to ~8.6 deg. Assuming an available time of ~18 (24) days[3] to map beams during Jupiter transits without violating the Sun aspect angle constraints, then the spin axis advance rate should be ~1.2 (0.9) arcmin per hour, allowing dense sampling with spin axis pointings separated by 0.5 arcmin.

This means that ~9.6 (12.8) days are used to map HFI near sidelobes (i.e. *U* in the approximate range [−0.04, 0.04]), and 4.8+7.2=12 (6.4+9.6=16) days are used to map LFI main beams (i.e. *U* in the approximate range [0.02, 0.06] and [−0.09,−0.03]). Note that 9.6+12=21.6 days >18 days (12.8+16=28.8 days > 24 days), since, clearly, different beams overlap in the *U* direction, as discussed above[4]. Note that for the same reason, these integration times are in line or even better that those discussed above (see Appendix E and section 6.1).

Case B: Only LFI is operational

Assuming that in January 2012 only LFI will continue to operate (and in general for subsequent Jupiter transits), we propose to map the whole relevant region of the *UV* plane with equal spacing along the *U*

[3] Celestial constraints analysis shows that the pointings before the start of the Jupiter scan (08/01/12) can be advanced by 1.5 days, and the pointings after the end of the Jupiter scan (30/01/12) can be delayed by 3 days. This means that 4.5 days-worth of Survey 5 pointings that would normally be performed during the Jupiter scan time will be recovered.

[4] These numbers can be easily rescaled, almost proportionally, if a different time is globally available for beam mapping through Jupiter transits.

direction in the range that can be efficiently split into the U range [−0.09, −0.025] and U range: [0.02, 0.06], corresponding to ~6 deg. Since the above two areas are separated by ~2.6 deg, they can be considered as separate deep annuli and consequently the total available time to map them, while satisfying Sun aspect angle constraints, is somewhat larger than considered in the previous case (although by a factor less than 2). The best choice to share the time between the two relevant regions is still to be determined.

Assuming an available time of ~24 days dedicated to map beams during Jupiter transits (for example 16 days at U<0 and 8 days at U>0), this implies a spacing of ~0.63 arcmin per hour.

E.4 Other planets

We have considered the information that could be extracted through the transits of other planets. For LFI, the only possibly relevant opportunities are represented by Mars and Saturn. In particular, given their peak signals (respectively, about 15 and 5 times smaller than that of Jupiter), it is unlikely that they will provide useful constraints on beam parameters.

Tests have been carried out using LFI DPC tools to verify whether Mars can yield any useful information, at least to monitor the locations of the beam centres in the telescope field of view. It is found that with Mars we could achieve a typical sensitivity of a few arcmin in the recovery of LFI beam centres, to be compared with current limits from Jupiter transits of the order of few arcsec. On the other hand Saturn, although 4-5 times less effective than Jupiter for beam centre determination (see Burigana et al. 2001), could be in principle considered to cross-check beam calibration, through long integrations during its transit in the LFI beams in June 2012, when thermal changes of *PLANCK* may produce measurable optical drifts. The pros and cons of this opportunity and, possibly, its implementation will be object of future investigations.

Appendix F: Crab Nebula as check/calibrator for the polarisation orientations

The Crab Nebula is our principle check/calibrator for the polarisation orientations of the *PLANCK* feed horns. As discussed in Leahy et al. (2010), in each pair of scan-aligned feed horns of the LFI, one is measured significantly better than the other.

After the double scan of the Crab in September 2012, each feed horn has scanned the Crab six times, with the scan angle (relative to ecliptic meridians) at –7.4° (3 times) 7.4° (twice) and –0.6° (once). All of these scans were in normal continuous scanning mode, i.e. with the spin-axis longitude advancing at about 2 arcmin/40 min, except for the last scan at –7.4°, which was in ‘catch-up’ mode at twice the normal speed. With all the data acquired to date, expected orientation errors on the three ‘bad’ 70 GHz feed horns are in the range 1.2°–1.4°. Also, the bad 44 GHz feed horn will still be uncertain to 0.84°, and the unpaired LFI-24 to 0.53°. All the other feeds already have orientation errors < 0.4°. These figures are all worse than the corresponding *WMAP* 7-year orientation uncertainties, despite the higher integrated sensitivity of the *PLANCK* 2-year maps compared to *WMAP*, because the crossing angles between the *PLANCK* scans is small compared to the optimal 45°.

While the current error level is adequate to separate E from B modes in LFI 3-year maps, it will dominate the uncertainty in the foreground polarisation angles at certain resolutions and galactic latitudes, and this in turn will reduce the legacy value of the LFI foreground polarisation maps, which may be used in the future for foreground removal from much higher-sensitivity data taken near 150 GHz (e.g. the COrE project, see The COrE Collaboration 2011).

Continuous scanning during the Warm Extension using any proposed scan pattern will give at best a modest (15%) reduction in the orientation errors, and the default plan of following the survey 5 scan strategy will give almost no improvement. We therefore plan deep ring observations to reduce all horn orientation errors to below 1° after the first deep-ring observations (March 2012), and to below 0.5° if the mission lasts long

enough to permit the second set of deep rings in September 2012 (see Table F.1). At 70 GHz, the deep rings have about 18 times the effective integration time of a continuous-scanning observation; at 44 GHz, a two-day ring is ~5 times deeper, because the larger beamwidth gives a longer effective observation in continuous scanning.

For effective constraints on the feed horn orientation, the scan angle must be moved away from the degenerate case (0°) which (almost) occurs in the 'smooth scanning' mode during the warm extension, viz. spin axis moving in a cycloid pattern with $\varphi_0 = 250°$. On the other hand, due to solar aspect constraints, the available spin axis longitude window shrinks to zero as the spin axis reaches the maximum allowed ecliptic latitude of just over 8°. At the epochs of potential Crab observations in March and September 2012, only solar constraints are important for spin axis latitudes below –5°. The proposed deep ring durations and spin axis latitudes are close to optimal in the sense of minimising the time needed to get errors below 0.5° after two deep scans (or one moderate-length scan in the case of LFI-24). Note that we cannot significantly reduce the orientation uncertainty after the March scan by simply increasing the time spent, since deep measurements are needed at two distinct scan angles.

The observations in September will need to be optimised, since a Jupiter visibility period is close to that of the Crab.

Horns	Month	Duration	Spin axis (λ,β) (degrees)	Orientation error (degrees)
LFI-25,26	March	2 days	(166.83,−7.50)	0.20, 0.64
LFI-18,23	March	3 days	(171.45, −6.60)	0.84, 0.15
LFI-19,22	March	3 days	(172.02, −6.60)	0.94, 0.14
LFI-20,21	March	3 days	(172.36, −6.60)	0.98, 0.13
LFI-24	March	0.5 day	(173.31, −6.60)	0.43
LFI-20,21	Sept	3 days	(355.85, −6.60)	0.47, 0.13
LFI-19,22	Sept	3 days	(356.17, −6.60)	0.46, 0.13
LFI-18,23	Sept	3 days	(356.74, −6.60)	0.41, 0.15
LFI-25,26	Sept	2 days	(1.37, −7.50)	0.20, 0.45

Table F1: Proposed Deep-ring observations of the Crab nebula. The Orientation Error column gives the error for all observations prior to and including the specified deep ring.

Appendix G: Low foreground regions vs deep scans

One of the advantages of the deep annuli scanning strategy was the possibility of identifying a limited set of deep annuli crossing sky areas with low foreground signal in polarisation. In those areas detailed analyses with LFI sensitivity similar to that of HFI would provide a better component separation on small sky areas at high multipoles. Clearly, the smooth scanning strategy cannot be optimised in this respect. In spite of this, it is interesting to verify where the deep annuli observed during the long integrations on calibration sources (Jupiter and Crab Nebula) are located in the sky. The result of this exercise is displayed in Fig. G1. Note that we are moderately lucky, since these deep annuli overlap with three patches of low foreground signal in

polarisation. Therefore, the deep annuli planned for Jupiter and Crab observations, as well as the polar caps where LFI gets naturally very deep sky patches, will be exploited for dedicated analyses, particularly for low foreground patches. In combination with HFI data, this will provide important information for small angular scales (high multipoles) investigations and, marginally, for deeper surveys of extragalactic sources in polarisation.

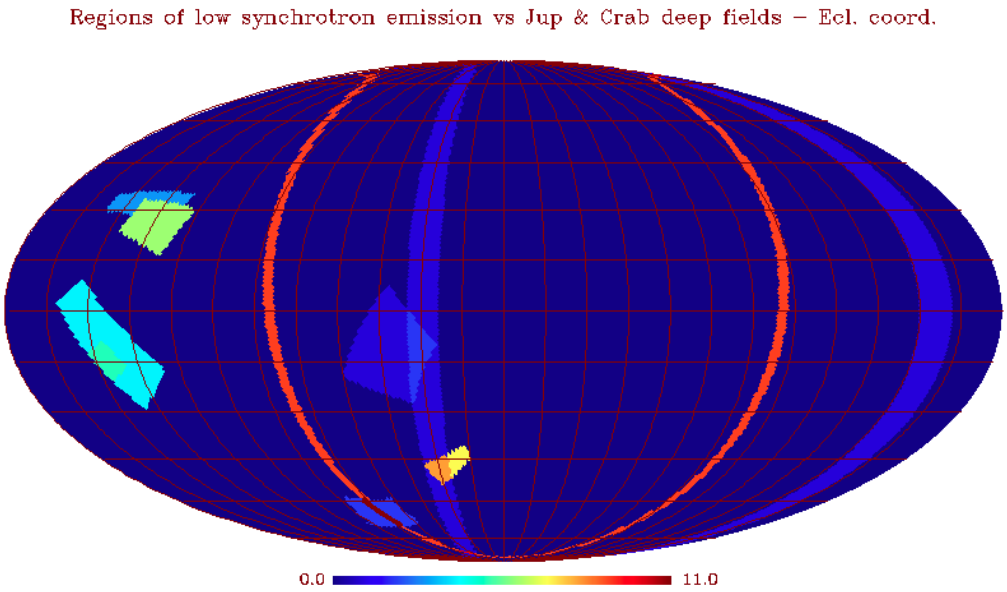

Fig. G1: Locations in the sky of various patches of particularly low polarised foreground emission derived on the basis of publicly available data (more accurate regarding the polarised synchrotron emission than regarding the polarised dust emission) compared with the deep annuli observed during the Jupiter transit in January 2012 (blue ring) and the Crab Nebula transit in March 2012 (red ring). The ring corresponding to the Crab Nebula transit in September 2012 is outside but very close to the edge of the patch observed in March. These results depend only very weakly on the considered beam. The color scale is arbitrary, its only meaning is that of distinguish among different sky patches and deep annuli.

Appendix H: Angular power spectra at low multipoles from simulated maps and using an optimal estimator

In this appendix we give details on the forecast measurements of the large angular scale polarisation with continuous scanning versus deep rings.

Given the importance of accurate measurements of the CMB polarisation spectra at low multipoles, we have used an optimal power spectrum estimator to compare the three scanning strategies discussed in Section 4, i.e.:

- Case 1: Surveys 1 to 5 (agreed programme up to expected end of HFI life);
- Case 2: Surveys 1 to 5 plus 6 months of Cycloidal coverage;
- Case 3: Surveys 1 to 5 plus 6 months of Deep Annuli coverage.

These cases are represented by three pixel-pixel noise covariance matrices presented in Appendix C. Here we restrict our attention to the 70 GHz channel, but similar results can be derived for 30

and 44 GHz.

For each case we evaluated the expected noise biases for all the six spectra, and the expected standard errors at each multipole as given by the diagonal elements of the inverse Fisher matrix. These estimates are obtained through a F90 implementation of the QML method (namely the *BolPol code*). Specifically, we have computed the following quantities (see Gruppuso et al. 2009 for more details on the formalism):

$$C_\ell^{nb,X} = \sum_{\ell',X'} \left(F^{X,X'}\right)^{-1}_{\ell\ell'} \mathrm{Tr}\left[NE_{\ell'}^{X'}\right]$$

$$SE = \left[\left(F_{\ell,\ell'}^{X,X'}\right)^{-1}\right]^{1/2}$$

where X,X' run over all kinds of spectra (*TT, EE, TE, BB, TB, EB*), ℓ is the multipole order, and F is the Fisher matrix defined as

$$F_{\ell,\ell'}^{X,X'} = \frac{1}{2}\mathrm{Tr}\left[C^{-1}\frac{\partial C}{\partial C_\ell^X}C^{-1}\frac{\partial C}{\partial C_{\ell'}^{X'}}\right],$$

while E is a matrix defined as

$$E_\ell^X = \frac{1}{2}C^{-1}\frac{\partial C}{\partial C_\ell^X}C^{-1}$$

where C is the covariance matrix in pixel space given by the sum of the signal and noise components, $C = S + N$.

In practice, the noise biases represent the power spectrum of the pixelised noise present in the maps. They are subtracted away in the process of estimating the power spectrum of the CMB, and they are a tracer of the amplitude of residual instrumental statistical noise. The SE above represent the fluctuations on the estimated spectra, due to both noise and signal (i.e. cosmic variance). These quantities are used as a figure of merit to evaluate the goodness of a given scanning choice.

The noise biases are plotted in the Fig. H1. We notice that there is an improvement going from Case 1 (orange lines) to the other cases because of the additional 6 months of observation of Case 2 (blue lines) or 3 (red lines). However the latter two cases have negligible differences from the point of view of noise level.

The same conclusion can be derived looking at Fig. H2, where we show the standard deviations computed through the Fisher matrix. . In these panels we display two sets of curves: the solid lines refer to the case in which the Covariance matrix appearing in the definition for the Fisher matrix is given by the sum $C=S+N$; the dotted lines correspond to the case $C=N$, i.e. neglecting cosmic variance. As for Fig. H1, we see that blue (case 2) and red (case 3) lines have negligible differences and both are better than the orange line (case 1) – as expected because of the additional 6 months of integration time.

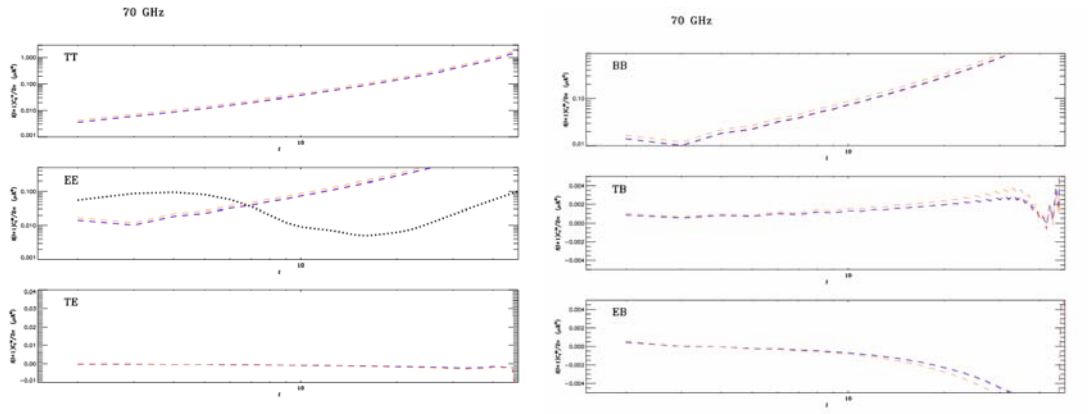

Fig. H1: Noise biases. Orange dashed line for Case 1, blue dashed line for Case 2 and red dashed line for Case 3. The dotted black line is the fiducial CMB model from WMAP-7.

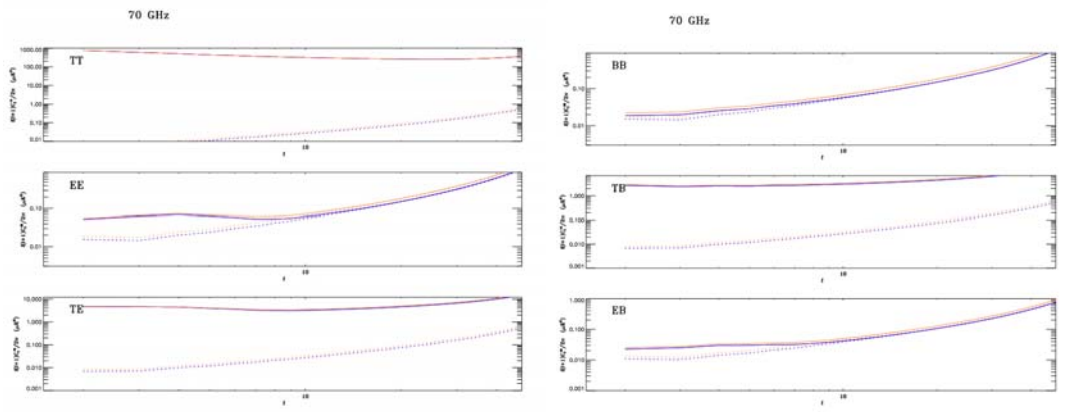

Fig. H2: Standard errors. Orange lines for Case 1, blue lines for Case 2 and red lines for Case 3. Solid lines are where the Fisher matrix is built considering $C=S+N$ and dotted lines are for the noise-only case, i.e. $C=N$.

The conclusion of this section is that from the current characterisation of the low resolution APS, case 2 and case 3 have negligible differences, as they are both dominated by the first 5 surveys, i.e. case 1. This indicates that the most relevant difference between the proposed scanning strategies for the extension is related to the knowledge and removal of systematic effects and related implications, rather than directly on the impact of statistical noise.

Appendix I: Evaluation of the impact of increasing the satellite spin rate for the LFI-only extension

We have evaluated the possibility to perform the LFI-extension survey with a 40% increased spin rate at 1.4 rpm. in order to minimise the impact of $1/f$ noise fluctuations and residuals. Our analysis (detailed in the annexed memo, Mennella et al. 2011) shows that any improvements in this respect are expected to be modest and comes the cost of increasing the sampling rate and, therefore, the LFI scientific telemetry rate which would require a retuning of the digital electronics box.

Furthermore the possibility to increase the spin rate and maintain it for the entire duration of the LFI extension survey is not guaranteed and the associated risks are not currently known.

For these reasons our conclusion is that we recommend to maintain the nominal spin rate throughout the extension survey.

Appendix L: Survey strategy to date

The first year of observations (surveys 1 & 2) followed the scan strategy described in Tauber et al. (2010a) (see also Dupac & Tauber 2005) in which the spin axis executes a 6-month period cycloid motion around the anti-Sun direction. This ensures coverage (multiple times) of the ecliptic pole regions at every frequency. The reference phase angle was chosen as $\phi_0 = 340°$, which maximises the scan crossing angle at the Crab nebula, thereby allowing us to use this highly-polarized source as our polarisation angle calibrator. The spin axis motion is not continuous but is stepped every 2 arcmin of ecliptic longitude, giving ~40 min of integration per scan circle. Observations in the second year (surveys 3 & 4) followed an almost identical scan pattern in order to allow clean jackknife comparisons to search for any secular changes in the instruments (the spin axis steps are interleaved with those of the first year to improve the sky sampling).

A well-understood drawback of the initial scan strategy is that every 90° in longitude all the scan paths are almost parallel or anti-parallel to the meridians (scan angle 0°). The lack of crossed scans in these regions slightly degrades our ability to remove the highest-frequency instrumental baseline terms, and also prevents us from recovering the spurious polarisation signal, since the *IQUSS* matrix that has to be inverted is singular when all scans are parallel. Consequently the fifth survey, started on July 29th 2011, shifted the cycloid phase a quarter-turn to 250°, which shifts the spin axis path 45° in longitude. This places the degenerate belts from the first pattern under the belts of maximum scan crossing angle from the second pattern, and vice versa. Since the Crab nebula suffers degenerate coverage in the second pattern, in September 2011 scanning briefly reverted to the original pattern to re-observe the Crab. As the simulations in Section 4 show, to reap the full benefit of the new scan pattern it needs to be in place for a full 12 months, i.e. throughout the sixth survey at least up to the expected end of 20-K sorption cooler operations, prior to any regeneration.

References

Bersanelli M., et al., 2010, A&A, 520, A4

Burigana C., Natoli P., Vittorio N., Mandolesi N., Bersanelli M., 2001, Exp. Astron., 12, 87

Dupac X., Tauber J., 2005, A&A, 430, 363

Gorsky K.M., Hivon E., Banday A.J., Wandelt B.D., Hansen F.K., Reinecke M., Bartelmann M., 2005, ApJ, 622, 759

Gruppuso A., et al., 2009, MNRAS, 400, 463

Keihänen E., Kurki-Suonio H., Poutanen T., Maino D., Burigana C., 2004, A&A, 428, 287

Leahy J.P., et al., 2010, A&A, 520, 8

Mandolesi N., et al., 2010, A&A, 520, A3

Mennella A., et al., 2011, Planck early results. III. First assessment of the Low Frequency Instrument in-flight performance, A&A, 536, id.A3

Mennella A., et al., 2011, Annexed Memo, "Evaluation of the impact of increasing the satellite spin rate for the LFI-only extension"

Page L., et al., 2007, ApJS, 170, 335

Pearson D., 2011, Cryo Operations Working Group, "Sorption Cooler Lifetime and Operations Status", Presentation 24 August 2011

Planck LFI Consortium, 2010, "LFI-only Extension Proposal" (LOEP)

Reinecke M., Dolag K., Hell R., Bartelmann M., Ensslin T., 2006, A&A, 445, 373

Seiffert M., Mennella A., Burigana C., Mandolesi N., Bersanelli M., Meinhold P., Lubin P., A&A, 391, 1185

Tauber J., et al., 2010a, A&A, 520, A1

Tauber J., et al., 2010b, A&A, 520, A2

The COrE Collaboration, 2001, "COrE (Cosmic Origins Explorer) A White Paper", arXiv:1102.2181

Zacchei A., et al., 2011, "Planck Early Results. V. The Low Frequency Instrument data processing", A&A, 536, id.A5